How to cite: *Angew. Chem. Int. Ed.* **2023**, *62*, e202219045
doi.org/10.1002/anie.202219045

Rotational Spectroscopy

Chiral Control of Gas-Phase Molecules using Microwave Pulses

Himanshi Singh[+], *Freya E. L. Berggötz*[+], *Wenhao Sun,* and Melanie Schnell**

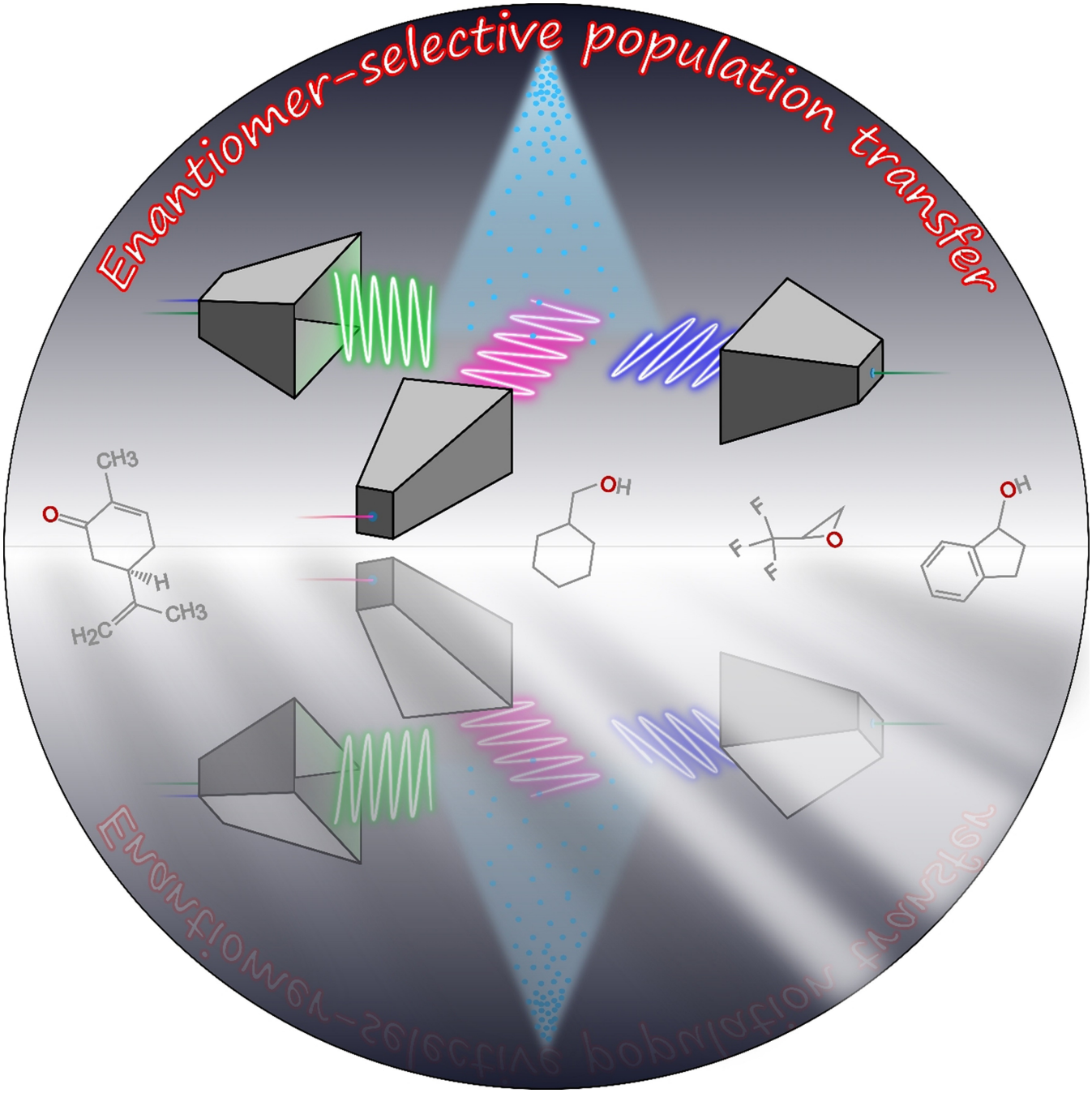

Abstract: Microwave three-wave mixing has emerged as a novel approach for studying chiral molecules in the gas phase. This technique employs resonant microwave pulses and is a non-linear and coherent approach. It serves as a robust method to differentiate between the enantiomers of chiral molecules and to determine the enantiomeric excess, even in complex chiral mixtures. Besides such analytical applications, the use of tailored microwave pulses allows us to control and manipulate chirality at the molecular level. Here, an overview of some recent developments in the area of microwave three-wave mixing and its extension to enantiomer-selective population transfer is provided. The latter is an important step towards enantiomer separation—in energy and finally in space. In the last section, we present new experimental results on how to improve enantiomer-selective population transfer to achieve an enantiomeric excess of about 40 % in the rotational level of interest using microwave pulses alone.

1. Introduction

Molecular chirality is an essential stereochemical property of molecular systems important in chemistry, biology, and medicine. Most biomolecules, such as amino acids, nucleic acids, and sugars, are chiral in nature and exist as a pair of non-superimposable mirror images called enantiomers. There is a stereoselective bias for biochemical interactions in different chemical or biological environments, which also expresses itself in the homochirality of life, whose origin is still highly debated to date.[1] Although the chemical and biological behaviors of the two enantiomers can vary dramatically in a chiral environment, their nearly identical physical properties, besides the extremely small energy difference arising from parity violation,[2,3] makes it intrinsically challenging to distinguish and separate them.

A powerful portfolio to differentiate between the enantiomers of chiral molecules has been developed, addressing chiral molecules in the solid state, the liquid or solution phase, and in the gas phase. Among those are X-ray diffraction, chirality-sensitive gas chromatography, polarimetry, and circular dichroism, to name a few.[4–7] In recent years, gas-phase spectroscopic techniques have emerged that allow for the analysis of chiral molecules with high resolution, free of solvent effects, bringing forward the ability to address the enantiomers of chiral molecules in an isomer- and conformer-selective way.[8,9] Furthermore, there is interesting progress to investigate chirality using ultrafast spectroscopy in the femtosecond to attosecond regime,[10–13] which gives access to ultrafast dynamics of chiral molecules, and in particular their electron dynamics.

These gas-phase techniques cover different ranges of the electromagnetic spectrum and thus address different molecular degrees of freedom. Photoelectron circular dichroism (PECD) has been shown to be able to differentiate between the enantiomers in simple chiral mixtures,[14–18] also in a conformer-selective way,[19,20] and it can be used to determine the enantiomeric excess (*ee*) with high precision.[21] This technique can be performed with synchrotron radiation[16,22–27] and nanosecond[28,29] up to femtosecond lasers so that also fast processes of the chiral molecules can be revealed.[30] It was also extended to photoelectron elliptical dichroism.[31] In another type of experiment, Coulomb explosion imaging of chiral molecules was performed, which allowed for the direct determination of the absolute configuration by calculating back the original structure.[32,33] Recently, the method could be applied to induce chiral fragmentation of a planar and thus achiral molecule upon interaction with helical light.[34,35] The outcome of the fragmentation, namely the observed fragment enantiomer, depends on the orientation of the molecule with respect to the light propagation direction and the helicity of the ionizing light. Moreover, enantioselective control of chiral molecular rotation using intense ultrashort laser fields has also been achieved experimentally,[36] following extensive theoretical demonstrations.[37–39] In addition to enantiomer differentiation, such gas-phase experiments also highlight their potential for separating, manipulating, and controlling chirality.

Another high-resolution gas-phase technique that will be central to this article is based on rotational spectroscopy and covers slower time scales and employs long-wavelength microwave radiation to excite molecules to quantized molecular rotational motions—microwave three-wave mixing (M3WM).[40,41] Since its first experimental implementation in 2013,[41,42] this M3WM technique, as a coherent, resonant, and non-linear approach, has showcased its capability and potential to control and manipulate chiral molecules. Microwave three-wave mixing has also inspired several theoretical studies and proposals on enantiomer differentiation and separation using optical fields.[43,44] In the following, we will discuss M3WM in more detail (Section 2) and then focus on its extension to generate enantiomer-selective population transfer. Using this extended transfer scheme, enantiomer excess in a rotational state of interest can be generated "on the fly" for a racemic starting sample

[*] H. Singh,[+] F. E. L. Berggötz,[+] Dr. W. Sun, Prof. Dr. M. Schnell
Deutsches Elektronen-Synchrotron DESY
Notkestr. 85, 22607 Hamburg (Germany)
E-mail: wenhao.sun@desy.de
melanie.schnell@desy.de
H. Singh,[+] Prof. Dr. M. Schnell
Institute of Physical Chemistry, Christian-Albrechts-Universität zu Kiel
Max-Eyth-Str. 1, 24118 Kiel (Germany)
F. E. L. Berggötz[+]
Institute for Experimental Physics, Universität Hamburg
Luruper Chausee 149, 22761 Hamburg (Germany)
[+] These authors contributed equally to this work.

of chiral molecules, which will be highly relevant for advanced experiments with chiral molecules, such as evaluating the frequency difference between the two enantiomers arising from parity violating weak interactions or enantiomer-selective collision studies.[45] The M3WM approach can be applied not only to permanently chiral molecules (e.g., carvone[46]) but also to transiently chiral species, such as benzyl alcohol,[47] where enantiomers can racemize due to quantum tunneling forming a racemic mixture, which is impossible to separate via conventional chemical methods. After reviewing some of the recent theoretical and experimental developments to improve enantiomer-selective population transfer, we report new experimental results to improve the efficiency of that scheme by the inclusion of a rapid adiabatic passage (RAP)- or a π-pulse.

2. Chiral analysis using high-resolution microwave spectroscopy

The analysis of chiral molecules with high-resolution microwave spectroscopy has developed into a powerful tool during the last years with different research applications and directions.[7,48–52] One particularly strong point is that the technique can be applied to the analysis of complex (chiral) mixtures due to its high resolution and fingerprint character for each molecule.[53,54] Once the rotational spectrum of a molecule is recorded, it can be unambiguously identified via its rotational transitions in later experiments. The narrow line widths on the order of 15–100 kHz (depending on the respective setup and frequency range applied) while covering several GHz of bandwidth in a single acquisition emphasize the potential of broadband rotational spectroscopy to record and identify several species at the same time. This was highlighted recently for the chiral analysis of essential oils, for example, which consist of numerous, structurally often very similar chiral compounds.[55]

Recently, two different approaches to analyse chiral samples using rotational spectroscopy have been developed: microwave chiral tagging[48] and microwave three-wave mixing.[7,41] In microwave chiral tagging, the sample of interest interacts with a well-characterized chiral tag molecule to form weakly bound complexes, resulting in diastereomers that can be differentiated via their structure.[7,48,52] By performing two different types of measurements, one with a racemic sample of the chiral tag molecule and one with an enantioenriched sample of known handedness for the tag, the excess enantiomer of the unknown sample as well as its corresponding enantiomeric excess can be determined with impressive statistics.[48,49,51,56,57]

While chiral tagging is experimentally more straightforward and thus promising as a routine application in chiral analysis, M3WM can additionally be applied to control and manipulate chiral molecules, which is the central part of this article.

2.1. Microwave three-wave mixing

M3WM is based on the mirror-image character of the two enantiomers of a chiral molecule, which results in opposite

Himanshi Singh obtained her BS-MS dual degree from the Indian Institute of Science Education and Research (IISER)-Mohali, India in 2019. She did her master's in the conformational study of alcohols using matrix isolation Fourier-transform infrared spectroscopy. Later, she joined the group of Prof. Melanie Schnell as a PhD student to explore high-resolution gas-phase spectroscopy. Her research interests are in studying molecular chirality and non-covalent interactions in flexible molecules using microwave spectroscopy.

Freya E. L. Berggötz obtained her Bachelor's degree in physics at the University of Hamburg, where she developed a setup to focus laser pulses in the extreme ultraviolet frequency range generated by a high harmonic source. Changing the field of research—and with it the frequency range—she later joined Prof. Melanie Schnell's group for her master's thesis to work on molecular chirality using microwave spectroscopy. After the successful completion of her thesis in 2021, she joined the group as a PhD student, continuing her work on molecular chirality.

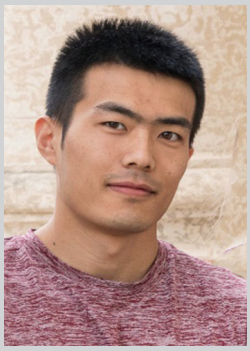

Wenhao Sun obtained his PhD at the University of Manitoba in Canada, where he studied sulfur-containing molecular species of astrophysical interest through rotational spectroscopy and discharge techniques under the supervision of Prof. Jennifer van Wijngaarden. Later he joined Prof. Melanie Schnell's group as a postdoctoral researcher. His present research focuses on the understanding of molecular chirality and weakly bound molecular complexes using rotational spectroscopy.

Melanie Schnell is professor for Physical Chemistry at the CAU Kiel and a leading scientist at DESY in Hamburg. Her research activities concentrate on a better understanding of chemical processes on the molecular level. To reach these goals, her group develops novel spectroscopic methods, with a focus on rotational spectroscopy. She received her PhD in physical chemistry with Jens-Uwe Grabow at the Universität Hannover. Following a research stay with Jon Hougen at NIST (Gaithersburg, USA), she joined the Fritz Haber Institute in Berlin before she moved to Hamburg in 2010 to set up her independent research group.

signs of the triple product of their transition dipole moments ($\vec{\mu}_a \cdot (\vec{\mu}_b \times \vec{\mu}_c)$) within the molecular principal axis system.[40–42,58] Furthermore, according to the selection rules for pure rotational transitions, each rotational transition of a molecule only depends on one particular dipole-moment component within the molecular principal axis system, i.e., μ_a, μ_b, or μ_c. The corresponding transitions are then denoted as a-, b-, and c-type transitions, respectively.

It is thus possible to selectively address the two enantiomers of a chiral molecule by generating an excitation cycle consisting of three rotational transitions, where each rotational transition involves only one of the three dipole-moment components in one particular direction of the laboratory frame (Figure 1). The molecular ensemble is excited by two consecutive resonant microwave pulses, for example polarizing an a- and a b-type transition, respectively, which are linearly polarized in two perpendicular directions of the laboratory frame. The first resonant pulse is optimized to fulfill the Rabi flip angle of π/2, corresponding to maximum coherence between the rotational states involved. The Rabi flip angle (Θ_{Rabi}) is defined as the product of the Rabi frequency, Ω_{Rabi}, and the pulse duration of the microwave pulse, τ:

$$\Theta_{Rabi} = \Omega_{Rabi} \cdot \tau = \frac{\mu \cdot E}{\hbar} \cdot \tau$$

where μ denotes the transition dipole moment for the rotational transition, E is the electric field amplitude. This π/2 pulse transfers the population difference between the two states $|1\rangle$ and $|2\rangle$ into coherence, and the associated transition is denoted as drive transition in Figure 1. As discussed in more detail below, it is advantageous to start with a large population difference of the two rotational states $|1\rangle$ and $|2\rangle$ connected by the drive transition, which will result in large coherence and which is supported by the usage of a supersonically expanded pulsed jet. Using neon as a carrier gas, rotational temperatures (T_{rot}) around 1–2 K are routinely achieved.[59] However, even at these low temperatures the population difference between levels $|1\rangle$ and $|2\rangle$ is still rather small due to the inherently small energy difference between rotational levels, so that thermal population is one of the limiting factors for efficient M3WM (and its extension to enantiomer-selective population transfer, see below).

The second pulse, the so-called twist pulse (Figure 1), is linearly polarized orthogonally to the direction of the drive pulse and is optimized for π conditions to transfer the coherence between states $|1\rangle$ and $|2\rangle$ induced by the π/2 drive pulse to the pair of states $|3\rangle$ and $|1\rangle$. This results in a molecular signal for this third transition, denoted as listen transition, which is linearly polarized in the third, mutually orthogonal direction. Note that this listen transition connecting states $|3\rangle$ and $|1\rangle$ is not directly excited by a resonant transition but is induced via the three-wave mixing scheme. The molecular signal at the frequency of the listen transition is recorded in form of a free-induction decay (FID) in the time domain that can be recorded in a phase-sensitive manner. The corresponding FID exhibits an opposite phase of π radians (180°) for the two enantiomers, which arises from the discussed opposite sign of the triple product of the three transition-dipole moments ($\vec{\mu}_a \cdot (\vec{\mu}_b \times \vec{\mu}_c)$), and it is the key to differentiating between the two enantiomers of chiral molecules via M3WM. The absolute phase provides information about the absolute configuration via the sign of ($\vec{\mu}_a \cdot (\vec{\mu}_b \times \vec{\mu}_c)$), while the calibrated intensity of the M3WM signal allows for the determination of the enantiomeric excess of the sample.[42,53,60,61] The former requires thorough knowledge of the timings of the excitation pulses and the listen signals traveling through the different electronic components of the instrument, which has been experimentally validated.[53,60] For a racemic sample, the two chiral signals destructively interfere so that no net signal is obtained at the frequency of the listen transition. As such, the technique is sensitive even to small *ee* values on the order of a few percent. Furthermore, M3WM is powerful to analyze also complex mixtures of chiral molecules because of its fingerprint character.[7,42,54,59] The handedness of the different chiral components can be analyzed simultaneously without any perturbations from the other chiral molecules in the sample, as shown in the case of essential oils.[54,55]

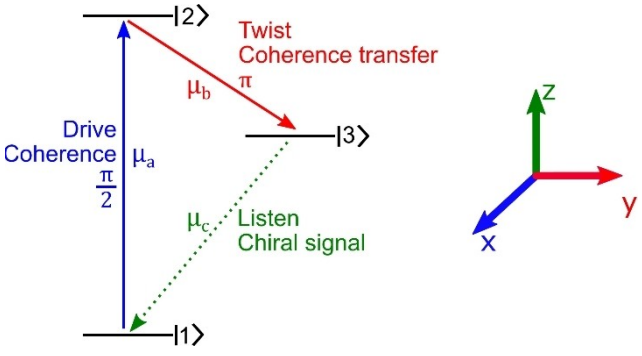

Figure 1. Generalized microwave three-wave mixing scheme consisting of drive transition (a-type, π/2-pulse, blue excitation), twist transition (b-type, π-pulse, red excitation), and listen signal (c-type, green detection). M_J degeneracies of the rotational energy levels are omitted here for clarity.

2.2. Enantiomer-selective population transfer using microwave three-wave mixing schemes

The phase difference of the two enantiomers generated for the FID of the listen transition can be used to enantiomer-selectively enhance the population of one enantiomer in a particular rotational state (and to deplete it in the connecting state of this transition), while the population of the second enantiomer will be depleted in this state but enhanced in the connecting state of the corresponding transition.[46,62–67] This enantiomer-selective population transfer is achieved by introducing a third pulse to the M3WM scheme, a so-called transfer pulse, which is resonant to the frequency of the listen transition, i.e., involving states $|1\rangle$ and $|3\rangle$, and which results in a direct excitation of this transition (Figure 2(a)). This direct excitation interferes with

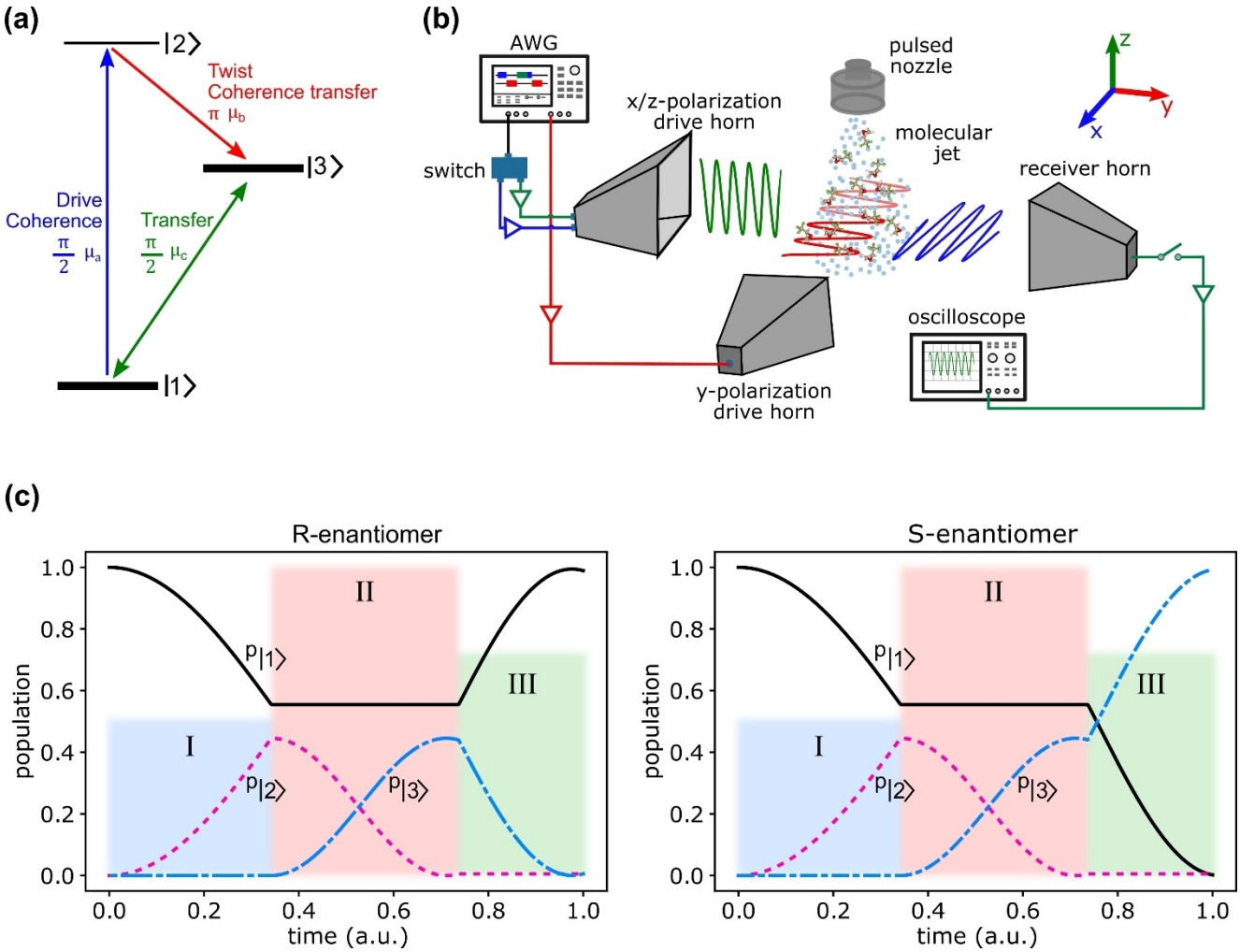

Figure 2. (a) Rotational energy level diagram for creating enantiomer-selective population transfer in the rotational levels $|1\rangle$ and $|3\rangle$ highlighted in bold. The created enantiomeric enrichment in the states $|1\rangle$ and $|3\rangle$ can be measured with any transitions connecting either state $|1\rangle$ or state $|3\rangle$. (b) Schematic of the Hamburg COMPACT spectrometer with relevant components and polarizations employed for performing M3WM or population transfer experiments. (c) Simulated enantiomer-selective population transfer for the R- and S-enantiomers in rotational states $|1\rangle$ and $|3\rangle$. Three pulses were applied subsequently (I: drive, II: twist, III: transfer), which enriched the R-enantiomer population in state $|1\rangle$ while the population of the S-enantiomer is enriched for state $|3\rangle$.

the phase-dependent listen signal induced by the M3WM scheme and converts the coherence into longer-lived population in states $|1\rangle$ and $|3\rangle$. Depending on the phase of the transfer pulse with respect to the M3WM scheme or the time delay in between, constructive or destructive interference between the two paths can be achieved, which is opposite for the two enantiomers as simulated in Figure 2(c) for the energy scheme shown in Figure 2(a). Thus, the populations of the two enantiomers are oppositely transferred to the rotational states $|1\rangle$ and $|3\rangle$, and chiral separation in energy is achieved.

This scheme has first been demonstrated using a buffer-gas cooled sample,[65] where 0.6 % enantiomeric enrichment was achieved (at $T_{rot} \approx 10$ K) and then, shortly after, it was realized for molecular jets with low rotational temperatures of 1–2 K, which allowed for an enhancement of the observed enantiomer-selective population transfer of one order of magnitude.[46] The effect was detected by determining the intensity change of an additional rotational transition as a probe involving either state $|1\rangle$ or state $|3\rangle$, respectively, as a function of the phase of the transfer pulse. The experiments for molecular jets were performed using the chirped-pulse Fourier transform microwave spectrometer COMPACT, modified for M3WM experiments (see Figure 2(b)), as reported elsewhere.[46,53,68]

Note that the handedness of the enantiomer enriched in a particular state (state $|1\rangle$ or state $|3\rangle$) only depends on the relative phase of the transfer pulse with respect to the pulses of the M3WM scheme. By changing one of the phases of the pulses involved by 180° (π radians), the type of enriched enantiomer for a respective energy level will be exchanged, while all other experimental conditions remain the same. Such experiments are thus not only of interest in their own rights, but they also deliver well-controlled starting samples for further advanced experiments on chiral molecules that depend on quickly changing the handedness of the enan-

tiomer without changing the experimental conditions, such as precision experiments, because systematic effects can be minimized.

In the first experiments, enrichment of one selected enantiomer in a particular rotational state (and the corresponding depletion of the other enantiomer) has been demonstrated for enantioenriched or even enantiopure samples as starting points,[65] and state-selective enantiomer enrichment on the order of a few percent could be achieved using our molecular jet.[46] In a follow-up experiment, we used cyclohexyl methanol (CHM) to demonstrate that this method can also generate an *ee* starting from a racemic sample.[66] CHM consists of two chiral conformers of opposite handedness; its interconversion is hindered by a barrier of about 15 kJ mol^{-1} as computed at the MP2/6-311++G(d,p) level of theory. At room temperature, the two enantiomers can rapidly interconvert, while they are stabilized at the cold conditions of a supersonic expansion. As such, they present an ideally racemic molecular ensemble to start with. Using an optimized enantiomer-selective population transfer scheme, state-specific enantiomeric excess starting from this racemic sample could be generated in a controlled way. Again, the enriched enantiomer could be switched and controlled by a π phase change of one of the pulses involved.

For these experiments, another read-out scheme needed to be applied to demonstrate the enantiomer selectivity of the approach and the resulting *ee* generated from a racemic sample. Instead of determining the intensity of a transition connecting to one of the states involved in the transfer process, we added a M3WM cycle to the population transfer scheme, starting from state $|3\rangle$ as shown in Figure 3(a). Since M3WM shows zero signal for a racemic mixture, the achieved *ee* could be sensitively detected. As shown in Figure 3(b), two maxima at the transfer-pulse phases of 126° and 306° were obtained, which could be shown to be corresponding to different enantiomers. The absolute configuration of the two maxima can in principle be determined with careful phase calibration as mentioned previously in Section 2.1, however, this is not a straightforward procedure.

2.3. Enhancing enantiomer-selective population transfer

Recent studies, both of theoretical and experimental nature, are focusing on increasing the efficiency of this approach. It depends on the difference in the thermal population as well as the spatial degeneracy of the rotational states involved, which is described by the quantum number M_J.[69,70] Phase variations due to field inhomogeneities are also a challenge, which can be circumvented to a good extent by using low excitation frequencies with wavelengths of several centimeters, so that field inhomogeneities are reduced. For example, a frequency at 5 GHz corresponds to a wavelength of about 6 cm. In the following, a short summary of the proposed and demonstrated improvement schemes will be given.

Each rotational energy level of an asymmetric top is denoted by J_{KaKc} and is $(2J+1)$-fold degenerate; the values of the M_J quantum number range from $-J, -J+1, \ldots, J-1, +J$. As a consequence, a simple pulse scheme as described above for M3WM (Figure 1) will result in several open cycles, reducing its efficiency. This effect is minimized for M3WM cycles involving $J=0$, for which only one M_J substate exists.[67,71] As theoretically derived in Ref. [71] using control theory applied to asymmetric tops, circularly polarized microwave radiation can increase the achieved enantiomer-

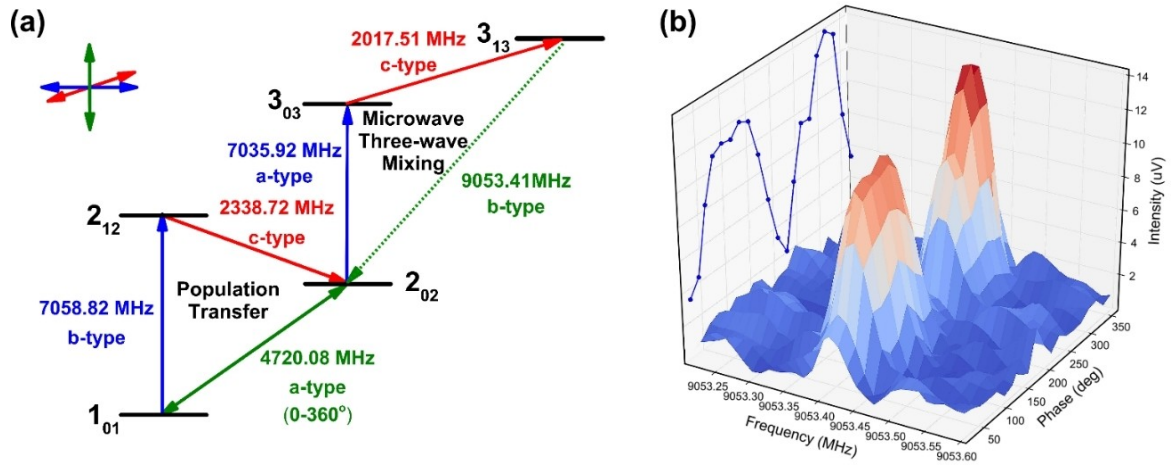

Figure 3. (a) Relevant rotational energy levels of cyclohexyl methanol (CHM) applied for state-specific enantiomeric enrichment. The rotational levels are denoted using the J_{KaKc} notation for an asymmetric top. The first set of triad creates an enantiomer-dependent population difference in the $|2_{02}\rangle$ and $|1_{01}\rangle$ rotational energy levels by varying the relative phase of the transfer pulse at 4720.08 MHz. This results in an opposite enantiomeric excess in both levels. The achieved enantiomeric excess in the rotational state $|2_{02}\rangle$ is then probed by the second cycle (M3WM) shown on the right. (b) The amplitude of the molecular signal of the listen signal at 9053.41 MHz was monitored as a function of the transfer pulse phase (0°–360° in 18° steps, 100,000 averages). Two maximal signals were observed, for the transfer pulse phases 126° and 306°, respectively. These two maxima correspond to the two enantiomers selectively populating or depopulating the $|2_{02}\rangle$ rotational level, creating an enantiomeric excess (*ee*). Figure adapted from Ref. [66] with permission. Copyright 2018 American Chemical Society.

selective enrichment from 6 % to about 8 % by including the cycles involving all M_J substates.

Since the overall M3WM signal and thus also the achieved population transfer via destructive or constructive interference between the M3WM signal and a direct excitation pulse depend on the population difference between the states involved, this is an important factor to consider. Because of the small energy difference between rotational states, the population difference is often also rather small, even at the cold conditions of a supersonic jet with rotational temperatures on the order of $T_{rot} \approx 1$–2 K or in a buffer-gas cell with temperatures around 8–10 K.

A large population difference can be achieved by involving a vibrational transition to a vibrationally excited state, as proposed in Ref. [70]. Recently, the population depletion of a rotational level involved in the M3WM scheme via electronic excitation from the S_0 to the S_1 state was demonstrated as shown in Figure 4, resulting in a significant efficiency increase.[67] Furthermore, the read-out was achieved via state-selective laser-induced fluorescence (LIF). This approach is predominantly applicable to the subset of chiral molecules that contain a UV chromophore, and it is thus an interesting additional tool for controlling chiral molecules.

In the following, we describe and demonstrate a general approach to significantly increase the efficiency of enantiomer-selective population transfer solely via rotational excitations, so that the additional requirement of a UV chromophore is not needed.

3. A general approach for enhancing enantiomer-selective population transfer using rotational excitation

As mentioned, the efficiency of enantiomer-selective population transfer is mainly limited by the M_J-degeneracy and the thermal population.[69,70] These limitations can be circumvented respectively by employing an energy level scheme involving low-lying rotational levels, such as the $|0_{00}\rangle$ rotational state, and by using controlled microwave pulse schemes to maximize the population differences between the initial states. The latter can be realized by exchanging the unwanted thermal population to a connected higher state prior to the population transfer experiment via: i) a resonant rotational excitation in the π-pulse regime on the Bloch sphere; or ii) a microwave chirp in the rapid adiabatic passage (RAP) regime.[72]

Here, we have explored the effect of both pulses on the enantiomer-selective population transfer for the molecule 2-trifluoromethyl oxirane (TFO), as demonstrated in Figure 5. Figure 5(b) illustrates the energy level scheme for achieving enantiomer-selective population transfer with TFO, which is adapted from the above-mentioned experimental scheme to separate the chiral conformers of cyclohexyl methanol.[66] A fast chirp in the RAP regime or a π-pulse (#6) is applied to invert the undesired thermal population in state $|1_{10}\rangle$ with the $|2_{11}\rangle$ rotational level, which is less populated. In this manner, the efficiency of the population transfer cycle can be enhanced, as it is proportional to the population difference between the $|1_{10}\rangle$ and $|0_{00}\rangle$ states. The following excitations of all three microwave pulses in the population transfer cycle induce an enantiomer-specific enrichment in states $|1_{01}\rangle$ and $|0_{00}\rangle$, which are opposite for the R- and S-enantiomers. The enantioenrichment is controlled by varying the phase of the transfer pulse and read out with a probe cycle. The enhancement of the achieved enantioenrichment is quantitatively assessed by directly comparing the results obtained with and without the π-pulse or RAP pulse. The experimental details are provided in the Supporting Information and are briefly described as follows.

Prior to performing the population transfer experiments, the durations of each of the excitation pulses were optimized for π/2 or π conditions on the Bloch sphere by recording the corresponding nutation curves. The results are presented in

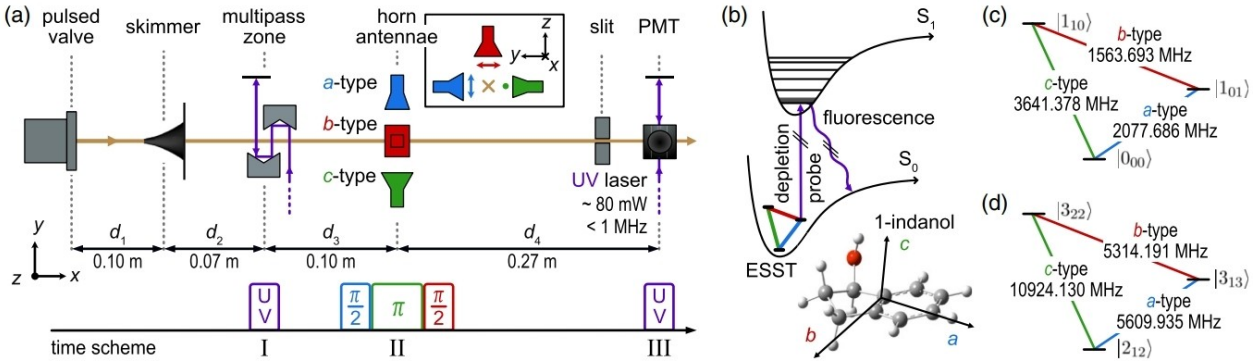

Figure 4. (a) Experimental setup, where jet-cooled 1-indanol is injected into the vacuum chamber through a pulsed valve. The molecules travel through a multi-pass zone where they interact with the UV depletion laser (step I). Further downstream, three microwave pulses with mutually orthogonal polarizations are applied for enantiomer-selective population transfer (step II). The molecules are interrogated by the same UV laser in the detection region, where the total laser-induced fluorescence intensity is measured with a photomultiplier tube (PMT) (step III). (b) Energy scheme consisting of electronic excitation and emission processes. The most stable conformer of 1-indanol is depicted together with the inertial axis system. (c + d) Energy-level schemes for two population-transfer cycles involved for 1-indanol. Figure is taken from Ref. [67] with Creative Commons Attribution 4.0 International license permission.

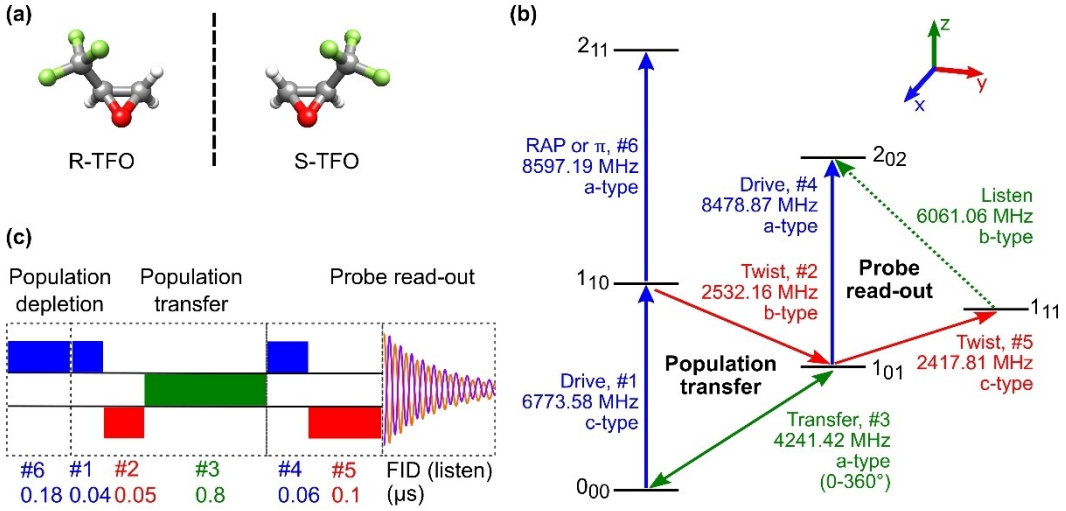

Figure 5. (a) Molecular structure of 2-trifluoromethyl oxirane (TFO) illustrating both enantiomers. (b) Rotational energy-level scheme for the coherent enantiomer-selective population transfer of TFO. The rotational levels are denoted using the J_{KaKc} notation. The color code indicates the polarization directions of the applied linearly polarized microwave fields (shown in Figure 2(b)). The population transfer cycle consisting of transitions #1, #2, and #3 creates an enantiomer-selective population difference between the $|0_{00}\rangle$ and $|1_{01}\rangle$ rotational levels. The selectivity can be controlled by varying the relative phase of the transfer pulse #3 at a frequency of 4241.42 MHz. This enantiomer enrichment is read out with a M3WM cycle (probe cycle) consisting of transitions #4, #5, and the listen transition (ν_L) at 6061.06 MHz. Pulse #6 is the preceding pulse applied to enhance the enantioenrichment, either as a rapid adiabatic passage (RAP) chirp or as a π-pulse. (c) Optimized pulse sequence in the time domain associated with the energy-level scheme in (b). Pulse #6 refers to either a π-pulse or a RAP-pulse of 4 MHz bandwidth.

Figures S2–S8 of the Supporting Information, and the optimal pulse conditions and durations are summarized in Table S2. The optimal five-pulse sequence for our experimental setup with a preceding pulse (pulse #6) is depicted in Figure 5(c). The pulses were fed in the respective mutually orthogonal polarizations using the dual-polarized horn antennas of the set-up shown in Figure 2(b). The color code in Figure 5 refers to the individual laboratory-fixed axes. The experiments were carried out with the racemic TFO sample, and the chiral signal of the probe cycle at the listen frequency ν_L (6061.06 MHz) yielded the created enantiomeric excess as a function of phase for the transfer pulse #3 (ϕ_3), at a frequency of 4241.42 MHz, varied from 0° to 360° in steps of 18°, while keeping the phases of pulse #1 and #2 constant.

More than 15,000 FID acquisitions were collected and averaged for each transfer phase. To assess the reproducibility of the observations, each set of experiments was repeated three times, which are provided in Figures S9–S11 in the Supporting Information. The same experiments were also performed with the enantiopure R- and S-TFO samples, which are used as the references with 100 % *ee*.

By comparison with the results from the enantiopure samples, the induced enantiomeric excess in the rotational state $|1_{01}\rangle$ from the racemic TFO mixture can be quantitatively determined using the following equation:

$$ee_{1_{01}} = \frac{I_L \cdot \gamma}{\frac{1}{2} \cdot [\langle I_{R,L}\rangle \cdot \gamma_R + \langle I_{S,L}\rangle \cdot \gamma_S]} \times 100\,\%$$

where I_L is the molecular response at the listen frequency (ν_L) when performing the enantiomer-selective population transfer experiment with the racemic TFO sample, $\langle I_{R,L}\rangle$, and $\langle I_{S,L}\rangle$ are the mean signal intensities at ν_L averaged over all phase steps throughout the population transfer experiments using the enantiopure R- and S-TFO samples. As the gas mixtures of racemic, R-, and S-TFO are prepared separately for the experiments, the respective concentrations of TFO are different. In each experiment, the mean signal intensity of the transfer transition (ν_3), which has the same polarization as the listen transition, is proportional to the concentration of TFO in the gas mixture and independent of the enantiomeric excess, thus it is used to normalize the results. In this equation, γ, γ_R, and γ_S are the normalization factors, which are the inverse of the mean intensity of the transfer transition (ν_3) obtained with racemic, R- and S-TFO samples, respectively, as summarized in Table S3 in the Supporting Information.

The overall results describing the created enantiomeric excess in the $|1_{01}\rangle$ rotational state from the racemic TFO sample are summarized in Figure 6(a) as a function of ϕ_3. The red, blue, and black curves show the results with and without the preceding π- or RAP-pulse. Two maxima at $\phi_3 =$ 90° and 270° were consistently observed in all experiments, corresponding to the maximum enantioenrichment in the $|1_{01}\rangle$ state. They are assigned to S- and R-TFO, respectively, by comparing the signal phases at ν_L with that obtained from the enantiopure samples, as shown in Figure S12 in the Supporting Information. Benefiting from the population transfer cycle starting with the ground state $|0_{00}\rangle$, an enantiomeric excess of about 13 % is obtained in the $|1_{01}\rangle$ state, which is twice of that reported with carvone (about 6 % in the $|2_{02}\rangle$ state).[46] With the implementation of the preceding π- or RAP-pulse prior to the population transfer

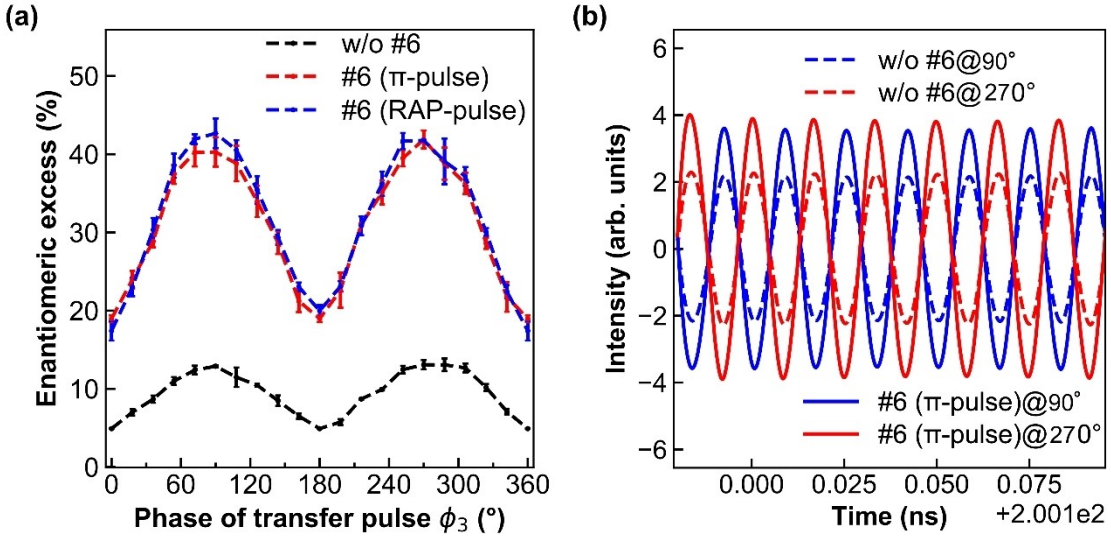

Figure 6. (a) The enantiomeric excess obtained for racemic TFO by applying the pulse sequence shown in Figure 5(c) is plotted as a function of the phase of the transfer pulse (ϕ_3), which was varied from 0° to 360° in steps of 18°. For each phase step, 15,000 FIDs were averaged and repeated three times. The errors are calculated from the three repeated experiments. The two maxima at $\phi_3 = 90°$ and 270° correspond to the maximum selective population transfer of the two enantiomers in the $|1_{01}\rangle$ rotational level. The black curve shows the enantiomer excess produced without any preceding pulse. The red and blue curves show the results with either a preceding π- or a RAP-pulse. (b) Portions of the free-induction decays (FIDs) at the listen frequency (ν_L) in the time domain with and without the preceding π-pulse when $\phi_3 = 90°$ and 270°. The phases of the obtained chiral signal at 90° and 270° show a shift of π radians, indicating the two different enantiomers in excess.

process, the induced *ee* is further improved to about 40 %, increasing the enantiomeric excess by about a factor of three.

In addition to the experiments, we simulated the enantiomeric enrichment in TFO using the QDYN program package developed by the group of Prof. Christiane Koch at the Freie Universität Berlin.[73] For this, we implemented the energy scheme for the population transfer cycle including all M_J states and the thermal population of the rotational states at a rotational temperature of 2 K. While using the experimentally determined pulse durations, the electric field strengths of all the pulses were optimized as shown in Table S4 of the Supporting Information. For each enantiomer, the initial thermal population was then numerically propagated with the optimized pulses, employing the Chebyshev expansion.[74] The *ee* in the rotational state $|1_{01}\rangle$ can be then obtained by subtracting the final populations of both the enantiomers in this state.

The phase dependence of the *ee* is simulated by scanning the phase ϕ_3 from 0° to 360°, as performed in the experiments. Figure 7 presents the simulated enantiomeric excess for the rotational state $|1_{01}\rangle$ with and without any preceding pulse. These simulated results agree qualitatively well with our experimental observations. The obtained quantitative differences between experiments and simulations can be accounted to differences in external factors such as different microwave field strengths used in the simulations than in our experiments.

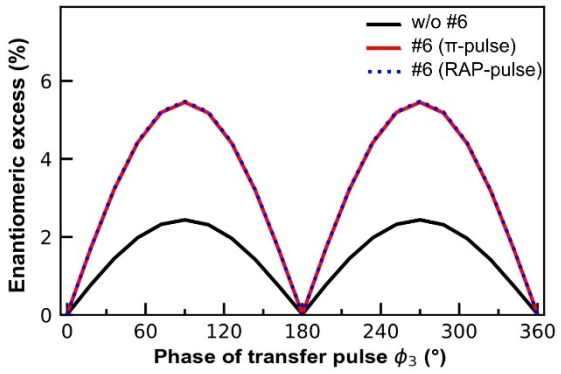

Figure 7. The simulated enantiomeric excess obtained for the rotational level $|1_{01}\rangle$ is plotted as a function of the phase of the transfer pulse #3, ϕ_3, using the program package QDYN.[73] The black curve represents the enantiomeric excess without a preceding pulse, while in red and blue the enantiomeric excess with either a preceding π- or RAP-pulse is shown.

4. Conclusions

The recent developments of chirality-sensitive techniques using gas-phase samples hold great promise for investigating and controlling chirality on different time scales and with different resolution. Approaches based on rotational spectroscopy can address chiral molecules even in complex chiral mixtures due to its fingerprint character.[7,42,54,59] With the recent development of the microwave three-wave mixing (M3WM) technique, which is a resonant, non-linear, and coherent approach, microwave spectroscopy can now be used to differentiate between enantiomers and to determine

their respective enantiomeric excess in complex chiral mixtures. The resonant nature of the technique has established a robust method to detect individual chiral components in mixtures such as peppermint oil.[55]

Advanced developments of M3WM demonstrate its ability to manipulate and control chiral molecules at the molecular level in the gas phase. Quantum-state separation of enantiomers and chiral purification are some of the ongoing challenges of chiral research. The ability to generate samples for which the excess enantiomer can be controlled and switched "on the fly" will be highly useful for advanced experiments with state-selected chiral molecules, such as chiral collisions or precision spectroscopy. A first step in that direction is discussed in section 2.2., where we have discussed how tailored microwave pulses can be used not only to read out the handedness of chiral molecules but also to promote enantioseparation. With the concept of coherent enantiomer state-selective population transfer, a particular enantiomer can be enhanced in a chosen rotational state compared to the other handedness. Recent work focuses on how to overcome the obstacles towards enhancing this state-specific enantioselective population transfer, which we summarize in section 2.3. of this minireview.

The effect of thermal population as a major factor can be reduced prior to the enantiomer separation and leads to significant enhancement in enantiomer enrichment. A recent work shows the use of a UV laser for depleting the target rotational state prior to the population transfer process and measuring the enantiomer enrichment with laser-induced fluorescence.[67] Here, we provide new experimental results for an enhanced enantiomer-selective population transfer scheme, which is based solely on microwave pulses, which makes it a general approach. With the usage of tailored microwave pulses such as π- and RAP-pulses, the effect of thermal population could be reduced and the enantiomeric excess achieved for a set of chosen rotational states could be increased by a factor of three compared to experiments without a population-inversion pulse, resulting in samples with 40 % enantiomeric excess of a chosen enantiomer in a specific rotational state starting from a racemic sample. These latest experiments on controlling the composition of a chiral sample in certain rotational states impressively demonstrate the level of control that can be achieved with high-resolution rotational spectroscopy and gas-phase samples.

Acknowledgements

We thank Dr. Denis S. Tikhonov for fruitful scientific discussions. We would also like to thank Prof. Christiane Koch, Dr. Monika Leibscher, and Alexander Blech for providing us with the QDYN program for performing simulations and for helpful discussions. This work has been supported by the collaborative linkage grant "Extreme light for sensing and driving molecular chirality (ELCH)", SFB 1319, of the Deutsche Forschungsgemeinschaft. Open Access funding enabled and organized by Projekt DEAL.

Conflict of Interest

The authors declare no conflict of interest.

Keywords: Chirality · Chirality Control · Coherent Excitation · Microwave Spectroscopy · Population Transfer

[1] A. Brandenburg, in *Prebiotic Chemistry and the Origin of Life* (Eds.: A. Neubeck, S. McMahon), Springer, Cham, **2021**, pp. 87–115.
[2] M. Quack, *Angew. Chem. Int. Ed.* **2002**, *41*, 4618–4630.
[3] M. Quack, J. Stohner, M. Willeke, *Annu. Rev. Phys. Chem.* **2008**, *59*, 741–769.
[4] K. W. Busch, M. A. Busch, *Chiral Analysis*, Elsevier, Amsterdam, **2006**.
[5] L. A. Nafie, *Vibrational Optical Activity: Principles and Applications*, Wiley, Chichester, **2011**.
[6] P. L. Polavarapu, *Chiroptical Spectroscopy*, CRC Press, Boca Raton, **2016**.
[7] B. H. Pate, L. Evangelisti, W. Caminati, Y. Xu, J. Thomas, D. Patterson, C. Perez, M. Schnell, in *Chiral Analysis* (Eds.: P. L. Polavarapu), Elsevier, Amsterdam, **2018**, pp. 679–729.
[8] K. Le Barbu, V. Brenner, P. Millié, F. Lahmani, A. Zehnacker-Rentien, *J. Phys. Chem. A* **1998**, *102*, 128–137.
[9] A. Zehnacker, Eds., *Chiral Recognition in the Gas Phase*, CRC Press, Boca Raton, **2010**.
[10] O. Smirnova, Y. Mairesse, S. Patchkovskii, *J. Phys. B* **2015**, *48*, 234005.
[11] R. Cireasa, A. E. Boguslavskiy, B. Pons, M. C. H. Wong, D. Descamps, S. Petit, H. Ruf, N. Thiré, A. Ferré, J. Suarez, J. Higuet, B. E. Schmidt, A. F. Alharbi, F. Légaré, V. Blanchet, B. Fabre, S. Patchkovskii, O. Smirnova, Y. Mairesse, V. R. Bhardwaj, *Nat. Phys.* **2015**, *11*, 654–658.
[12] S. Beaulieu, A. Comby, A. Clergerie, J. Caillat, D. Descamps, N. Dudovich, B. Fabre, R. Géneaux, F. Légaré, S. Petit, B. Pons, G. Porat, T. Ruchon, R. Taïeb, V. Blanchet, Y. Mairesse, *Science* **2017**, *358*, 1288–1294.
[13] D. Ayuso, A. F. Ordonez, P. Decleva, M. Ivanov, O. Smirnova, *Opt. Express* **2022**, *30*, 4659–4667.
[14] H. G. Breunig, G. Urbasch, P. Horsch, J. Cordes, U. Koert, K. M. Weitzel, *ChemPhysChem* **2009**, *10*, 1199–1202.
[15] P. Horsch, G. Urbasch, K. M. Weitzel, *Chirality* **2012**, *24*, 684–690.
[16] C. Lux, M. Wollenhaupt, T. Bolze, Q. Liang, J. Köhler, C. Sarpe, T. Baumert, *Angew. Chem. Int. Ed.* **2012**, *51*, 5001–5005.
[17] U. Boesl, A. Bornschlegl, C. Logé, K. Titze, *Anal. Bioanal. Chem.* **2013**, *405*, 6913–6924.
[18] M. H. M. Janssen, I. Powis, *Phys. Chem. Chem. Phys.* **2014**, *16*, 856–871.
[19] G. A. Garcia, H. Soldi-Lose, L. Nahon, I. Powis, *J. Phys. Chem. A* **2010**, *114*, 847–853.
[20] G. A. Garcia, H. Dossmann, L. Nahon, S. Daly, I. Powis, *Phys. Chem. Chem. Phys.* **2014**, *16*, 16214–16224.
[21] A. Kastner, C. Lux, T. Ring, S. Züllighoven, C. Sarpe, A. Senftleben, T. Baumert, *ChemPhysChem* **2016**, *17*, 1119–1122.
[22] N. Böwering, T. Lischke, B. Schmidtke, N. Müller, T. Khalil, U. Heinzmann, *Phys. Rev. Lett.* **2001**, *86*, 1187–1190.
[23] G. A. Garcia, L. Nahon, M. Lebech, J. C. Houver, D. Dowek, I. Powis, *J. Chem. Phys.* **2003**, *119*, 8781–8784.
[24] U. Hergenhahn, E. E. Rennie, O. Kugeler, S. Marburger, T. Lischke, I. Powis, G. Garcia, *J. Chem. Phys.* **2004**, *120*, 4553–4556.
[25] I. Powis, C. J. Harding, G. A. Garcia, L. Nahon, *ChemPhysChem* **2008**, *9*, 475–483.

[26] G. A. Garcia, L. Nahon, S. Daly, I. Powis, *Nat. Commun.* **2013**, *4*, 2132.
[27] L. Nahon, L. Nag, G. A. Garcia, I. Myrgorodska, U. Meierhenrich, S. Beaulieu, V. Wanie, V. Blanchet, R. Géneaux, I. Powis, *Phys. Chem. Chem. Phys.* **2016**, *18*, 12696–12706.
[28] A. Kastner, T. Ring, H. Braun, A. Senftleben, T. Baumert, *ChemPhysChem* **2019**, *20*, 1416–1419.
[29] S. T. Ranecky, G. B. Park, P. C. Samartzis, I. C. Giannakidis, D. Schwarzer, A. Senftleben, T. Baumert, T. Schäfer, *Phys. Chem. Chem. Phys.* **2022**, *24*, 2758–2761.
[30] D. S. Tikhonov, A. Blech, M. Leibscher, L. Greenman, M. Schnell, C. P. Koch, *Sci. Adv.* **2022**, *8*, eade0311.
[31] A. Comby, E. Bloch, C. M. M. Bond, D. Descamps, J. Miles, S. Petit, S. Rozen, J. B. Greenwood, V. Blanchet, Y. Mairesse, *Nat. Commun.* **2018**, *9*, 5212.
[32] M. Pitzer, M. Kunitski, A. S. Johnson, T. Jahnke, H. Sann, F. Sturm, L. P. H. Schmidt, H. Schmidt-Böcking, R. Dörner, J. Stohner, J. Kiedrowski, M. Reggelin, S. Marquardt, A. Schießer, R. Berger, M. S. Schöffler, *Science* **2013**, *341*, 1096–1100.
[33] P. Herwig, K. Zawatzky, M. Grieser, O. Heber, B. Jordon-Thaden, C. Krantz, O. Novotný, R. Repnow, V. Schurig, D. Schwalm, Z. Vager, A. Wolf, O. Trapp, H. Kreckel, *Science* **2013**, *342*, 1084–1086.
[34] K. Fehre, S. Eckart, M. Kunitski, M. Pitzer, S. Zeller, C. Janke, D. Trabert, J. Rist, M. Weller, A. Hartung, L. P. H. Schmidt, T. Jahnke, R. Berger, R. Dörner, M. S. Schöffler, *Sci. Adv.* **2019**, *5*, eaau7923.
[35] K. Fehre, S. Eckart, M. Kunitski, C. Janke, D. Trabert, M. Hofmann, J. Rist, M. Weller, A. Hartung, L. P. H. Schmidt, T. Jahnke, H. Braun, T. Baumert, J. Stohner, P. V. Demekhin, M. S. Schöffler, R. Dörner, *Phys. Rev. Lett.* **2021**, *126*, 083201.
[36] A. A. Milner, J. A. M. Fordyce, I. MacPhail-Bartley, W. Wasserman, V. Milner, I. Tutunnikov, I. S. Averbukh, *Phys. Rev. Lett.* **2019**, *122*, 223201.
[37] A. Yachmenev, S. N. Yurchenko, *Phys. Rev. Lett.* **2016**, *117*, 033001.
[38] E. Gershnabel, I. S. Averbukh, *Phys. Rev. Lett.* **2018**, *120*, 083204.
[39] I. Tutunnikov, E. Gershnabel, S. Gold, I. S. Averbukh, *J. Phys. Chem. Lett.* **2018**, *9*, 1105–1111.
[40] E. Hirota, *Proc. Jpn. Acad. Ser. B* **2012**, *88*, 120–128.
[41] D. Patterson, M. Schnell, J. M. Doyle, *Nature* **2013**, *497*, 475–477.
[42] D. Patterson, J. M. Doyle, *Phys. Rev. Lett.* **2013**, *111*, 023008.
[43] J. L. Wu, Y. Wang, S. L. Su, Y. Xia, Y. Jiang, J. Song, *Opt. Express* **2020**, *28*, 33475–33489.
[44] F. Zou, Y. Y. Chen, B. Liu, Y. Li, *Opt. Express* **2022**, *30*, 31073–31085.
[45] A. Lombardi, F. Palazzetti, *J. Phys. Condens. Matter* **2018**, *30*, 063003.
[46] C. Pérez, A. L. Steber, S. R. Domingos, A. Krin, D. Schmitz, M. Schnell, *Angew. Chem. Int. Ed.* **2017**, *56*, 12512–12517.
[47] W. Sun, D. S. Tikhonov, H. Singh, A. L. Steber, C. Pérez, M. Schnell, *Nat. Commun.* **2023**, *14*, 934.
[48] L. Evangelisti, W. Caminati, D. Patterson, J. Thomas, Y. Xu, C. West, B. Pate, **2017**, Talk RG03, *The 72nd International Symposium on Molecular Spectroscopy*, Urbana-Champaign, https://dx.doi.org/10.15278/isms.2017.RG03.
[49] M. D. Marshall, H. O. Leung, K. Wang, M. D. Acha, *J. Phys. Chem. A* **2018**, *122*, 4670–4680.
[50] S. R. Domingos, C. Pérez, M. Schnell, *Annu. Rev. Phys. Chem.* **2018**, *69*, 499–519.
[51] S. R. Domingos, C. Pérez, M. D. Marshall, H. O. Leung, M. Schnell, *Chem. Sci.* **2020**, *11*, 10863–10870.
[52] M. D. Mills, R. E. Sonstrom, Z. P. Vang, J. L. Neill, H. N. Scolati, C. T. West, B. H. Pate, J. R. Clark, *Angew. Chem. Int. Ed.* **2022**, *61*, e202207275.
[53] V. A. Shubert, D. Schmitz, D. Patterson, J. M. Doyle, M. Schnell, *Angew. Chem. Int. Ed.* **2014**, *53*, 1152–1155.
[54] V. A. Shubert, D. Schmitz, M. Schnell, *J. Mol. Spectrosc.* **2014**, *300*, 31–36.
[55] A. Krin, M. M. Quesada Moreno, C. Pérez, M. Schnell, *Symmetry* **2022**, *14*, 1262.
[56] K. Mayer, C. West, F. E. Marshall, G. Sedo, G. S. Grubbs, L. Evangelisti, B. H. Pate, *Phys. Chem. Chem. Phys.* **2022**, *24*, 27705–27721.
[57] F. Xie, N. A. Seifert, A. S. Hazrah, W. Jäger, Y. Xu, *ChemPhysChem* **2021**, *22*, 455–460.
[58] J.-U. Grabow, *Angew. Chem. Int. Ed.* **2013**, *52*, 11698–11700.
[59] S. Lobsiger, C. Perez, L. Evangelisti, K. K. Lehmann, B. H. Pate, *J. Phys. Chem. Lett.* **2015**, *6*, 196–200.
[60] V. A. Shubert, D. Schmitz, C. Medcraft, A. Krin, D. Patterson, J. M. Doyle, M. Schnell, *J. Chem. Phys.* **2015**, *142*, 214201.
[61] D. Patterson, M. Schnell, *Phys. Chem. Chem. Phys.* **2014**, *16*, 11114–11123.
[62] M. Shapiro, P. Brumer, *Adv. At. Mol. Opt. Phys.* **2000**, *42*, 287–345.
[63] P. Král, M. Shapiro, *Phys. Rev. Lett.* **2001**, *87*, 183002.
[64] P. Král, I. Thanopulos, M. Shapiro, D. Cohen, *Phys. Rev. Lett.* **2003**, *90*, 033001.
[65] S. Eibenberger, J. Doyle, D. Patterson, *Phys. Rev. Lett.* **2017**, *118*, 123002.
[66] C. Pérez, A. L. Steber, A. Krin, M. Schnell, *J. Phys. Chem. Lett.* **2018**, *9*, 4539–4543.
[67] J. Lee, J. Bischoff, A. O. Hernandez-Castillo, B. Sartakov, G. Meijer, S. Eibenberger-Arias, *Phys. Rev. Lett.* **2022**, *128*, 173001.
[68] D. Schmitz, V. A. Shubert, T. Betz, M. Schnell, *J. Mol. Spectrosc.* **2012**, *280*, 77–84.
[69] K. K. Lehmann, *J. Chem. Phys.* **2018**, *149*, 094201.
[70] M. Leibscher, T. F. Giesen, C. P. Koch, *J. Chem. Phys.* **2019**, *151*, 014302.
[71] M. Leibscher, E. Pozzoli, C. Pérez, M. Schnell, M. Sigalotti, U. Boscain, C. P. Koch, *Commun. Phys.* **2022**, *5*, 110.
[72] V. S. Malinovsky, J. L. Krause, *Eur. Phys. J. D* **2001**, *14*, 147–155.
[73] C. Koch, A. Blech, D. Basilewitsch, M. Goerz, F. Krack, "QDYN - quantum dynamics and control," can be found under https://qdyn-library.net/, **2020** (accessed on 22 December 2022).
[74] A. Gil, J. Segura, N. M. Temme, in *Numerical Methods for Special Functions*, Society for Industrial and Applied Mathematics, Philadelphia, PA, **2007**, pp. 51–86.

Manuscript received: December 23, 2022
Accepted manuscript online: March 3, 2023
Version of record online: April 27, 2023